Silicon Resonant Cavity Enhanced Photodetector Arrays for Optical Interconnects

M. K. Emsley[*a], O. I. Dosunmu[a], P. Muller[b], M. S. Unlu[a], Y. Leblebici[b]
[a]Electrical and Computer Engineering, Boston University, 8 Saint Mary's Street, Boston, MA 02215
[b]Electrical Engineering, Swiss Federal Institute of Technology, 1015 Lausanne, Switzerland

ABSTRACT

High bandwidth short distance communications standards are being developed based on parallel optical interconnect fiber arrays to meet the needs of increasing data rates of inter-chip communication in modern computer architecture. To ensure that this standard becomes an attractive option for computer systems, low cost components must be implemented on both the transmitting and receiving end of the fibers. To meet this low cost requirement silicon based receiver circuits are the most viable option, however, manufacturing high speed, high efficiency silicon photodetectors presents a technical challenge. Resonant cavity enhanced (RCE) Si photodetectors have been shown to provide the required bandwidth-efficiency product and we have recently developed a method to reproduce them through commercially available fabrication techniques. In this work, commercially reproducible silicon wafers with a 90% reflectance buried distributed Bragg reflector (DBR) are used to create Si-RCE photodetector arrays for optical interconnects. The Si-RCE photodetectors have 40% quantum efficiency at 860 nm, a FWHM of 25 ps, and a 3dB bandwidth in excess of 10 GHz. We also demonstrate Si-RCE 12x1 photodetector arrays that have been fabricated and packaged with silicon based amplifiers to demonstrate the feasibility of a low cost monolithic silicon photoreceiver array.

Keywords: Photodetector, photodiode, resonant cavity enhanced, RCE, SOI, optical interconnect, photoreceiver

1. INTRODUCTION

Optical interconnects represent the future of not only the telecommunications industry, but also the entire computing industry. It may sound like a bold statement, the computing industry has been getting along quite well for decades, but a simple look at the numbers will tell the story. Figure 1 shows the growth in bandwidth for CPU's and the peripheral bus.

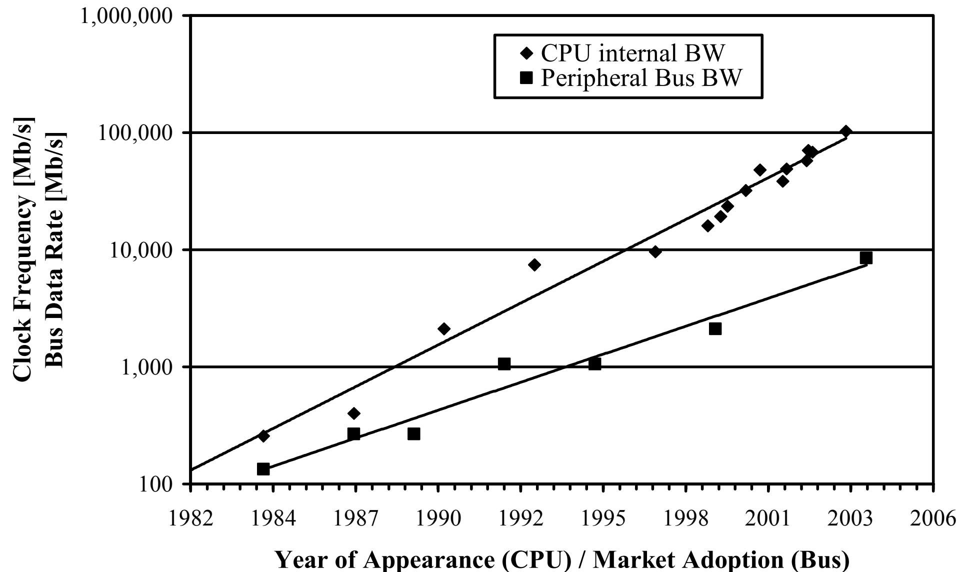

Fig. 1. CPU and peripheral bandwidth increase over time

*memsley@bu.edu; phone 1 617 353 1712; fax 1 617 353-9917

It is clear that for the past two decades a chasm has been opening between the two. One can consider the processing power of a computer to be inherently serial in nature, combining input/output (I/O) and CPU speeds. When I/O lags CPU speed by an order of magnitude, the computational throughput of the computer is no longer determined by the CPU. In this situation the CPU becomes a commodity within computer architecture, which is clearly something that Intel has strived to avoid for many years.

The telecommunications industry has made huge investments in the long-distance high bandwidth links that can carry terabits of information, but fiber to the home remains elusive and many people still use dial-up modem access. An interesting point is that data can be sent 3,000 miles across the Atlantic Ocean in less time then it takes to go the 3 inches from the memory to the processor. Paul Green wrote in the December issue of IEEE Spectrum, *"Both computers and the common carriers' systems run at multiple tens of gigabits per second. Dial-up modems carry, at best, 50 kb/s – nowhere near enough to support the innovative new services on which the future prosperity of both the telecom and computer industries depends."* [1]

What is needed is a high speed data link for short haul communications. There are several standards being developed to satisfy the short haul communication traffic jam. These so-called optical interconnects are based on arrays of laser transmitters coupled with similar arrays of photodetector receivers coupled through low cost plastic optical fiber arrays. One such standard being developed is Infiniband based on a 12x1 array of parallel optical interconnects operating at 2.5 Gbps per channel.

Since there are many more downstream computers than upstream nodes there is an intense effort to develop low cost components. Owing to the low cost drive, 850 nm light sources are utilized due to the low cost of plastic optical fiber as well as the lower cost of 850 nm vertical cavity surface emitting lasers (VCSEL). On the receiving end III-V semiconductors are the current standard due to the optimum efficiency, but a serious effort to develop low cost alternatives has not been pursued until recently. One reason for this is that the relative cost of the photodetector compared to the laser has focused the effort towards reducing cost of the more expensive lasers. Market conditions have recently arisen, however, that make finding lower cost alternatives attractive in both the transmitters and the receivers.

On the receiving end there has been an intense effort to develop Si based photodetectors [2]. It has been the standard in semiconductors that silicon based devices have always been lower in cost. The reason for this is quite simple; InP, currently the standard for high speed photodiodes, is available in wafer sizes typically 3" in diameter, while Si wafers are available in 12" diameters. This corresponds to a square millimeter cost of a few orders of magnitude less for Si than InP. There are also the fabrication costs which are inherently less for Si due to the overwhelming size of the Si processing industry, but also due to the simple fact that fewer wafers have to be fabricated because of the difference in area. Unfortunately for the industry, silicon exhibits poor optical absorption efficiency due to its indirect band gap, thus requiring long absorption path lengths. The long absorption length adversely affects the device bandwidth as in a typical device the contacts sandwich the absorption region, and carriers generated in this region must traverse to the contacts. The longer the distance between the contacts the longer it takes for all the carriers to be collected. Table 1 shows a comparison of commercially available InGaAs/InP based photodetectors and a Si photodetector. Also listed in Table 1 is the Si-Resonant Cavity Enhanced (RCE) photodetector that has been fabricated in this work.

Table 1: Parameters for commercially available InGaAs and Si high speed photodetectors and results from Si-RCE that we fabricated

Parameter	Unit	InGaAs (70 μm) [3]	Si [4]	Si-RCE (70 μm)
Responsivity, R	A/W	0.45 (λ=830 nm)	0.35 (λ=780 nm)	0.32 (λ=780 nm)
Dark Current, I_D	nA	10	0.02	3 pA
Capacitance, C	pF	0.5	2	0.2
Bandwidth, B	GHz	5	<1	3.5
Bias Voltage, V^+	V	2	2	2

As is shown in Table 1 standard Si photodetectors have lower responsivity and much lower bandwidth and would be unable meet the specifications of the optical interconnect standards. It can also been seen however, that Si-RCE photodetectors come quite close in performance, and have an order of magnitude lower dark current, which is a typical advantage of Si over III-V devices.
It is prudent to stress the following points: 1) Si based photodetectors offer the ability to monolithically integrate detectors and receivers. 2) Standard Si photodetectors offer inadequate device performance. 3) Si-RCE photodetectors offer desirable performance.

Resonant cavity enhanced (RCE) photodetectors have been shown to provide the required bandwidth-efficiency product but have remained a challenge to reproduce through commercially available fabrication techniques. We have previously developed a method to produce silicon wafers with high reflectance buried distributed Bragg reflectors (DBR) [5]. The substrates consist of a two-period, 90% reflecting, DBR fabricated using a double silicon-on-insulator (SOI) process. Discrete Si-RCE photodetectors have previously been fabricated with 40% quantum efficiency at 860 nm, a FWHM of 25 ps, and a 3dB bandwidth in excess of 10 GHz [6].

2. PHOTODETECTOR FABRICATION

Si-RCE *p-i-n* photodetectors were fabricated in the epitaxial device layer, which was approximately 2.1 μm in total thickness, using standard Si device fabrication techniques. The device structure is shown schematically in Fig. 2. The structure has a buried n+ implant and a p+ implant on the surface, while the epitaxial Si layer is left undoped yielding the vertical *p-i-n* diode. Below the device layer is the two period DBR creating a Fabry-Perot cavity; with the Air/Si interface acting as the top reflector.

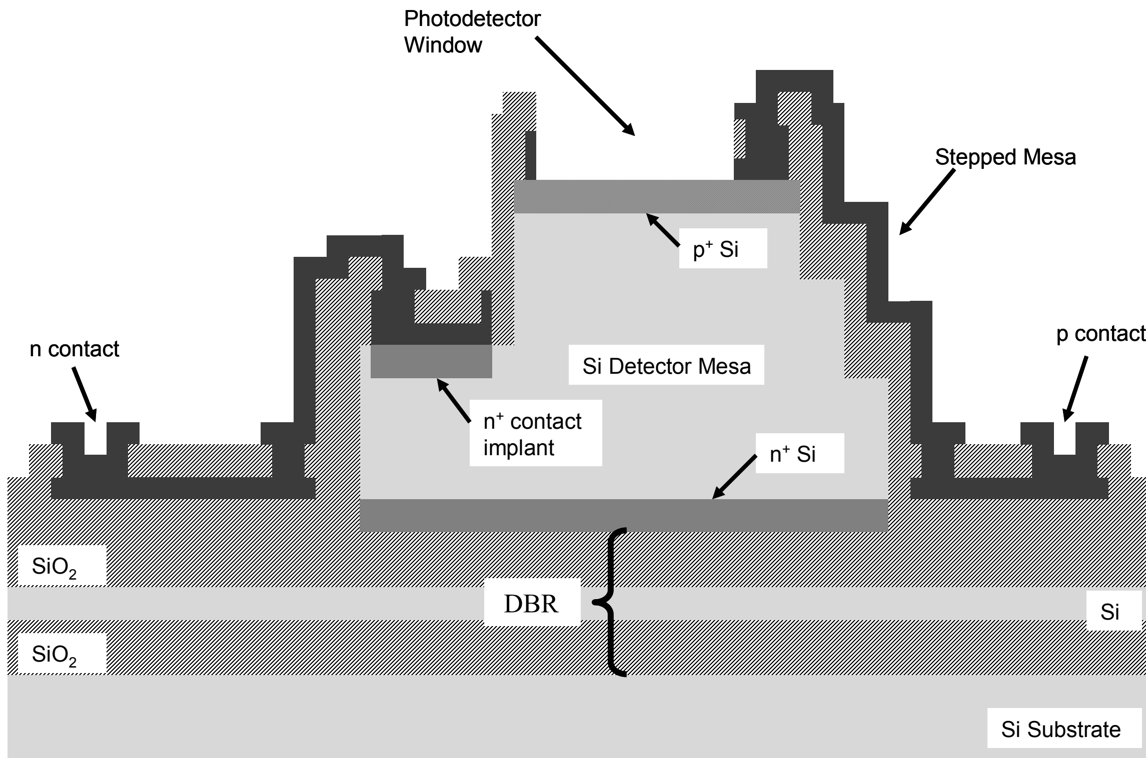

Fig. 2. Cross-section of Si-RCE p-i-n photodetector

In this paper we present Si-RCE 12x1 photodetector arrays that have been fabricated and packaged with silicon based amplifiers to demonstrate the feasibility of a low cost monolithic silicon photoreceiver array. The 12x1 photodetector arrays were designed for the PAROLI product line specification by Infineon [7]. The specification calls for 12 photodetectors with between 30 and 80 μm photodetector active area in a linear array on a 250 μm pitch. The fabricated 12x1 photodetector array can be seen in Fig. 3.

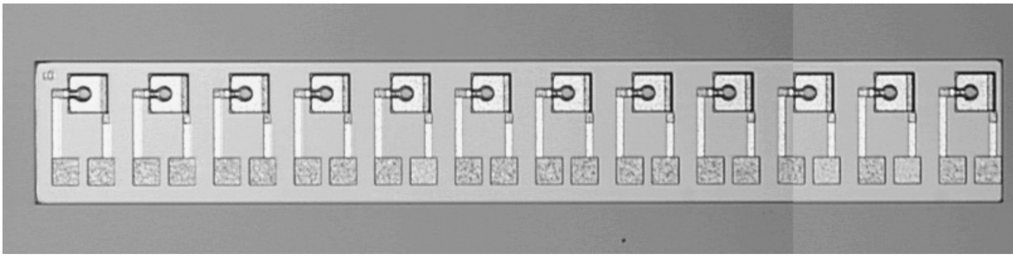

Fig. 3 Parallel 12x1 photodetector array

3. RESULTS AND DISCUSSION

3.1. I-V Characteristics

After fabrication, the photodetectors' I-V characteristics were measured using an HP4156A Parameter Analyzer. I-V measurements were done on two rows of photodetectors randomly selected from one wafer. These discrete photodetectors range in diameter from 22 μm to 200 μm. The I-V characteristic of the 200 μm diameter photodetector can be seen in Fig. 4.

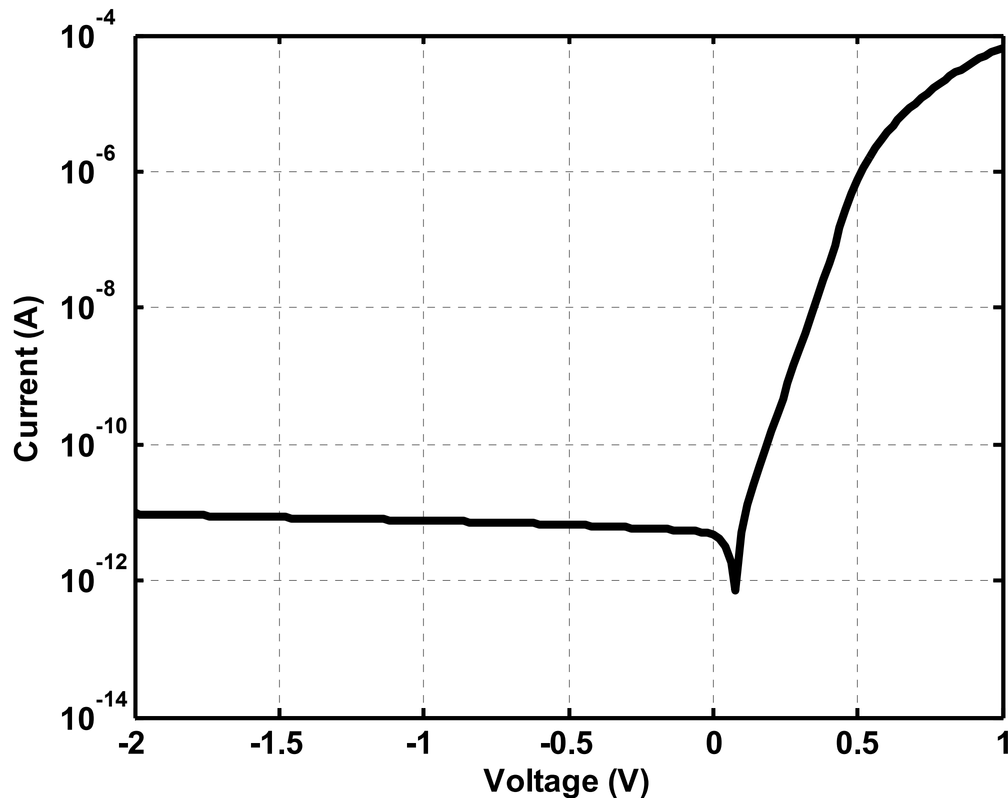

Fig. 4 I-V characteristic for 200 μm diameter device

Excellent reverse voltage characteristics were observed with all devices having less than 10 nA of current with 35 V of applied bias. The reverse voltage characteristic for the 200 μm diameter photodetector can be seen in Fig. 5.

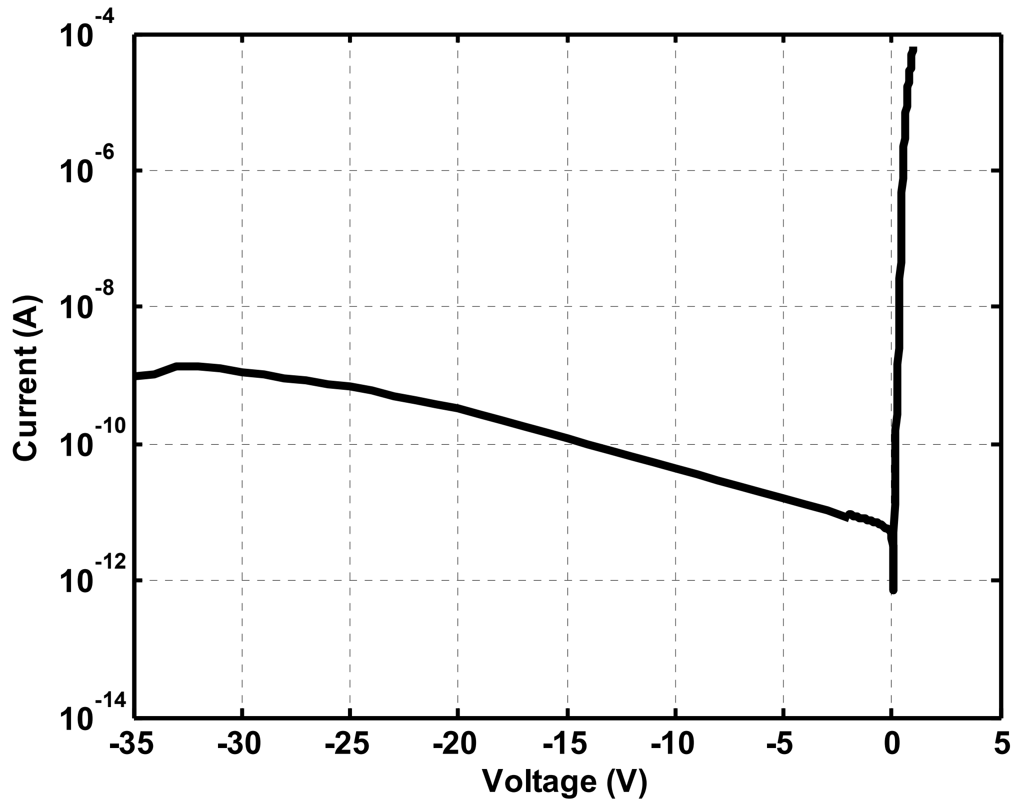

Fig. 5 I-V curve for 200 μm diameter device showing current increase as a function of bias

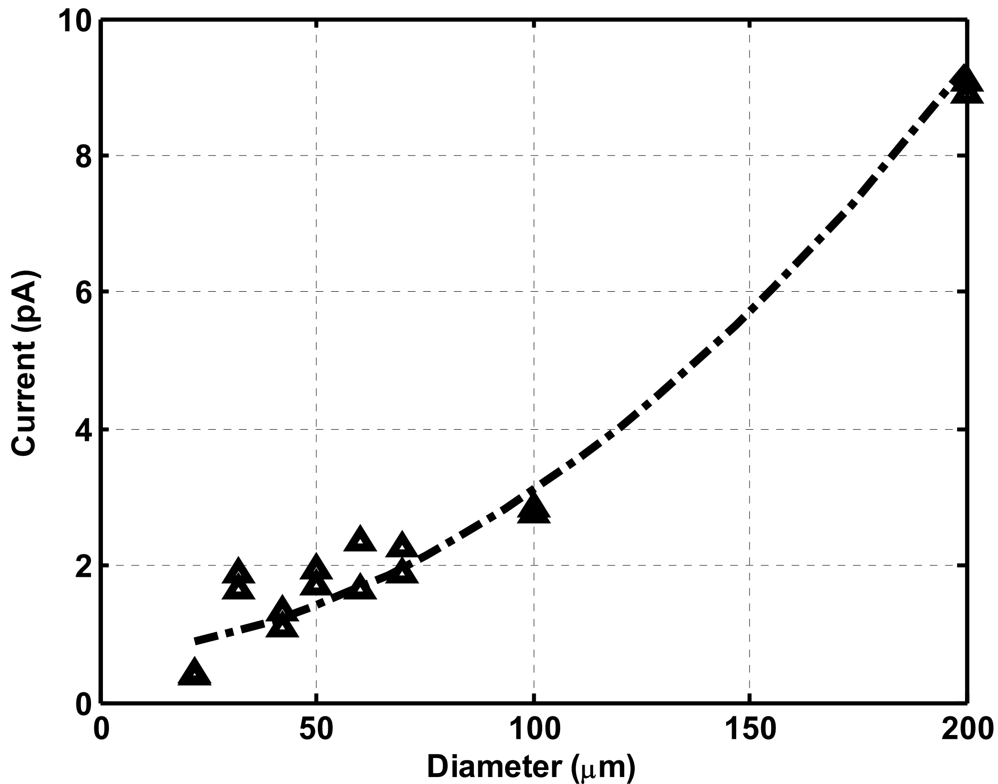

Fig. 6 Current at 1.8 V reverse bias as function of diameter showing square dependence

The dark current on 200 μm–diameter photodetectors was measured as 9 pA or 29 nA/cm^2 at reverse bias of 1.8 V, which is the bias voltage used in receiver testing discussed later. On 22 μm–diameter devices, the dark current density measured 105 nA/cm^2 at the same bias level. The decrease in dark current density from smaller to larger devices can be explained by reduced parallel diode output resistance for larger area devices. Fig. 6 shows the dark current at 1.8 V reverse bias as a function of device diameter with the fit line showing square dependence on diameter, or as expected the dark current is primarily a linear function of area.

3.2. Quantum Efficiency

Spectral quantum efficiency measurements were performed using a tunable Ti:Sapphire laser source and a calibrated, NIST traceable, Si photodetector with known spectral responsivity for photocurrent normalization. A reference scan was performed with the calibrated Si photodetector to determine the optical power at the test point as a function of wavelength. The RCE photodetector was then put in place of the calibrated photodetector and the current is measured as a function of wavelength. Knowing the current from the detector and power from the light source gives the responsivity of the photodetector. Lock-in amplifiers were also used to reduce noise from external light sources.

It can be seen from Fig. 7 that the spectral responsivity agrees well with the simulation and that the responsivity near 822 nm is approximately 0.30 A/W, which is roughly 40% quantum efficiency. It is also evident in Fig. 7 that the peak wavelength does not occur at 850nm, which is due to a slightly thick top Si layer. Spectral tuning can be achieved by recessing the top Si thickness, [8], although this was not performed during this study. The discrepancy between the measured and simulated responsivity peaks is presumed to be measurement error.

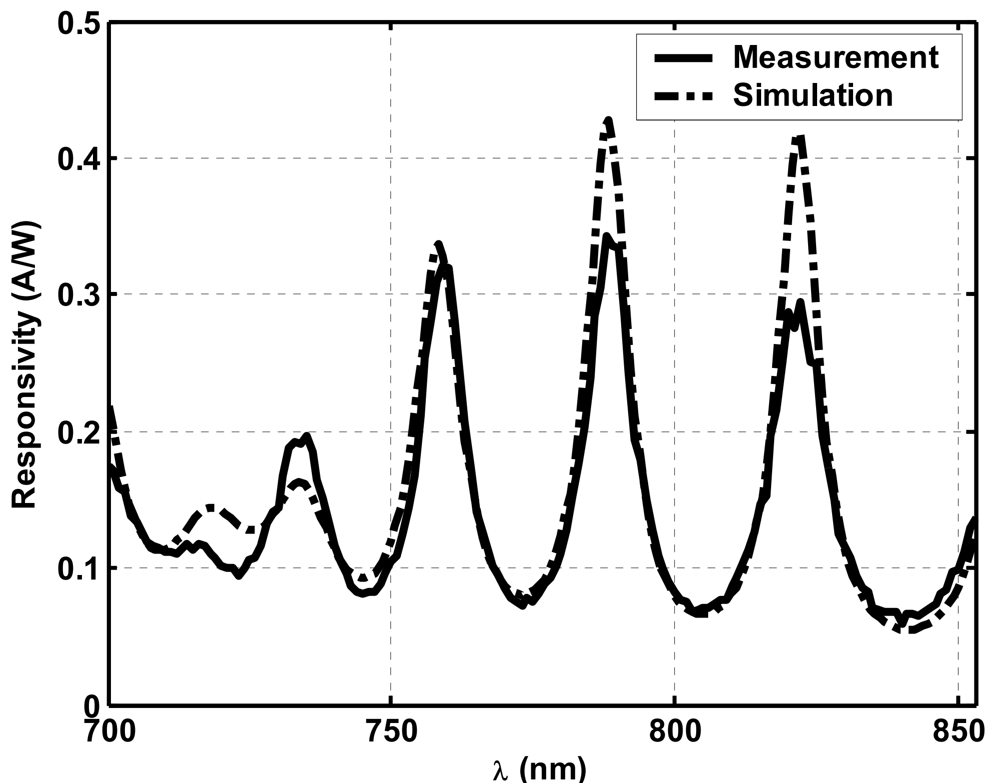

Fig. 7. Spectral quantum efficiency of RCE p-i-n photodetector

3.3. Temporal Response

High-speed characterization was performed on a Karl Suss PM5 microwave probe station using a Hewlett Packard 54750A Digitizing Oscilloscope with a HP-54753A TDR Module for monitoring the trigger signal and HP-54752A two

channel 50GHz Module for measuring the device under test (DUT). The device was probed with a Ground-Signal-Ground Picoprobe Model #67A-GSG-150-LP Serial #19276 from GGB Industries, Inc. Thorlabs High-Speed Photodetector Model #SV2-FC Serial #2138 served as the trigger for doing the sampling measurement and was connected to the HP-54752A external trigger input. A Spectra Physics Tsunami Ti:Sapphire Picosecond Laser was used to perform impulse response measurements on the photodetectors. The Spectra Physics laser emits approximately a 1.5 ps full-width at half-maximum (FWHM) pulse with a repetition rate of 83 MHz. The sampling scope took 4096 samples of the device response and was stored on a computer. The devices were biased using a Hewlett Packard 4156A Precision Semiconductor Parameter Analyzer and a 470 Ω resistor in series with the photodetector to limit the current.

Fig. 8 shows the temporal response obtained at 3 V reverse bias from a 22 μm diameter photodetector with measured FWHM value of 24.8 ps. The device had a rise time of 12 ps and a fall time of 44 ps. The FWHM of 24.8 ps suggests a bandwidth above 10 GHz, which is well beyond the requirements for 10 Gbps data communications.

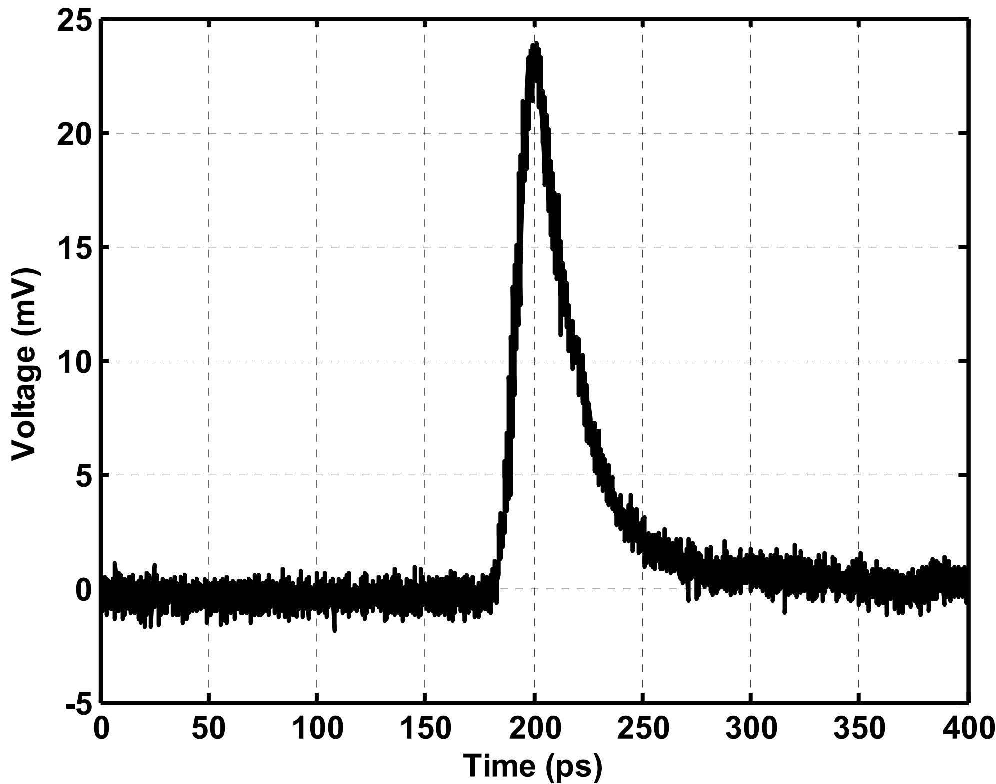

Fig. 8. Measured temporal responses of 22 μm-diameter device at 3 V reverse bias

3.4. Frequency Response

To study the frequency response, measured temporal response data for various size devices at different bias values were converted to frequency domain using fast Fourier transform (FFT) as shown in Fig. 9. A 4096 point FFT was performed on the sampled data. The data was sampled with two different window lengths to achieve a low resolution, long time scale FFT and a high resolution short time scale FFT. Window lengths of 10ns and 400ps were used to give a 100 MHz minimum frequency and an improved noise performance from 2.5 GHz, respectively, through the 3dB limit of the probe setup of 35 GHz. Fig. 9 shows the 3 dB bandwidth obtained from a 22 μm-diameter photodetector at 4 V reverse bias.

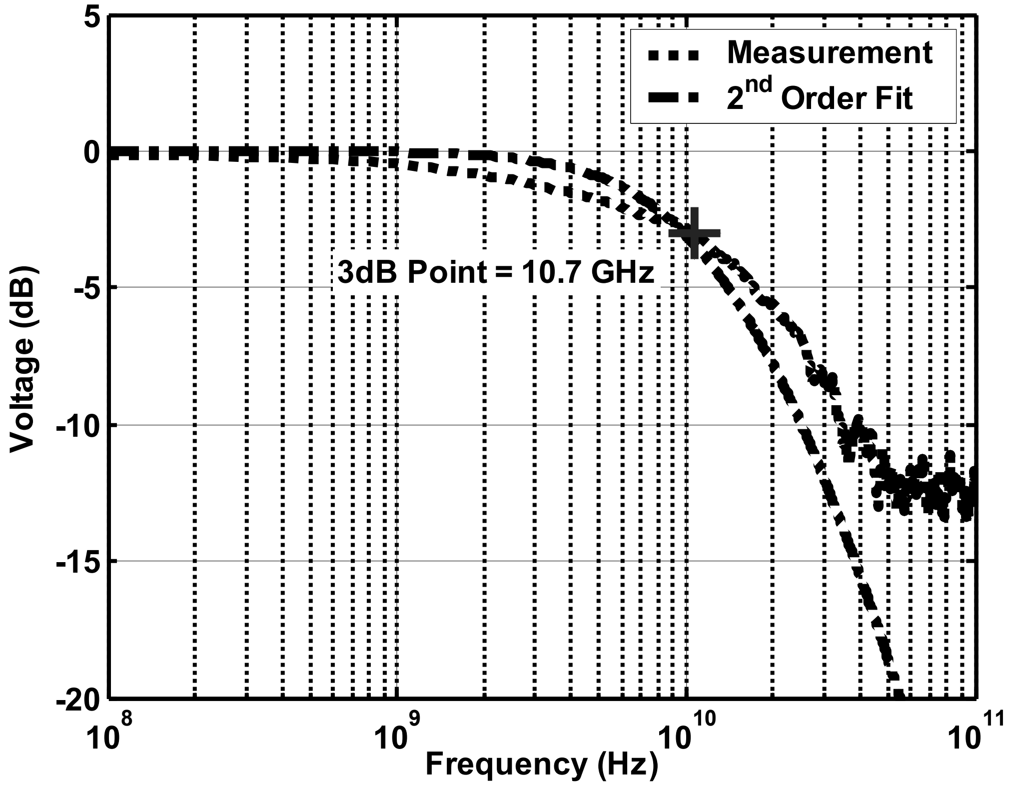

Fig. 9. FFT of Temporal Response for 22 μm-diameter photodiode at 4 V reverse bias

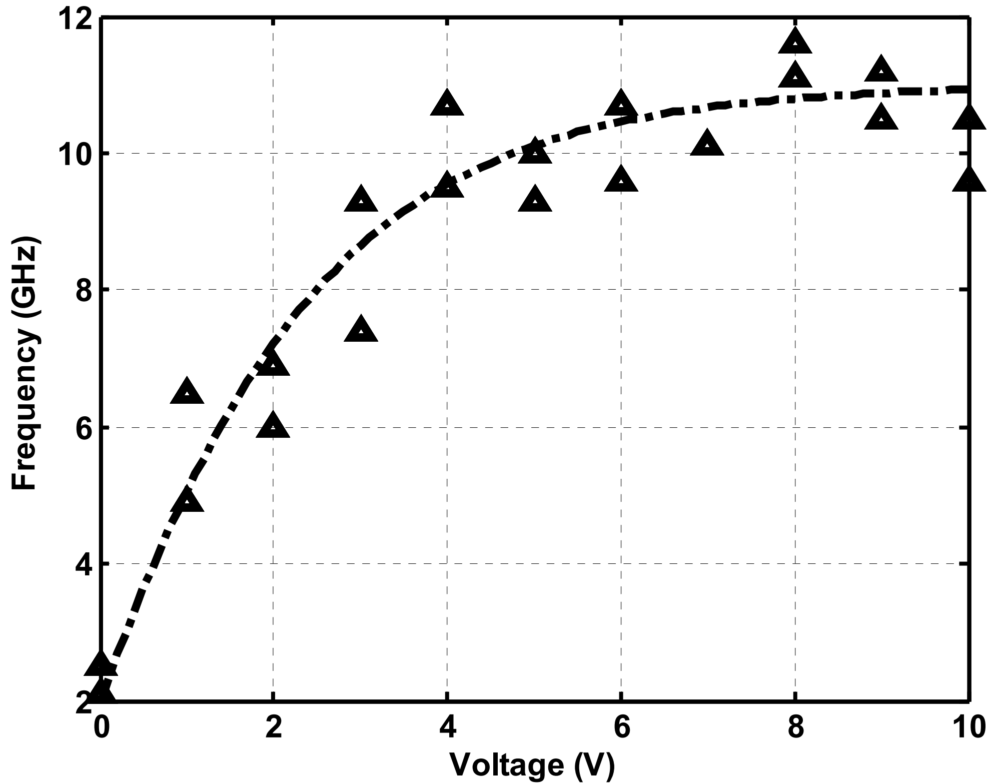

Fig. 10. 3dB Bandwidth as function of bias voltage for two 22 μm-diameter photodiodes (with trend line)

Temporal responses were measured at different reverse bias voltage to determine the 3dB frequency dependence on bias voltage. Devices were tested with bias voltage ranging from 0 V to 10 V in 1 V increments.
Fig. 10 shows the 3dB frequency as a function of voltage for two randomly selected 22 μm diameter photodetectors. Figure 11 shows the frequency response for photodetectors ranging in size from 22 μm to 200 μm at 10 V reverse bias.

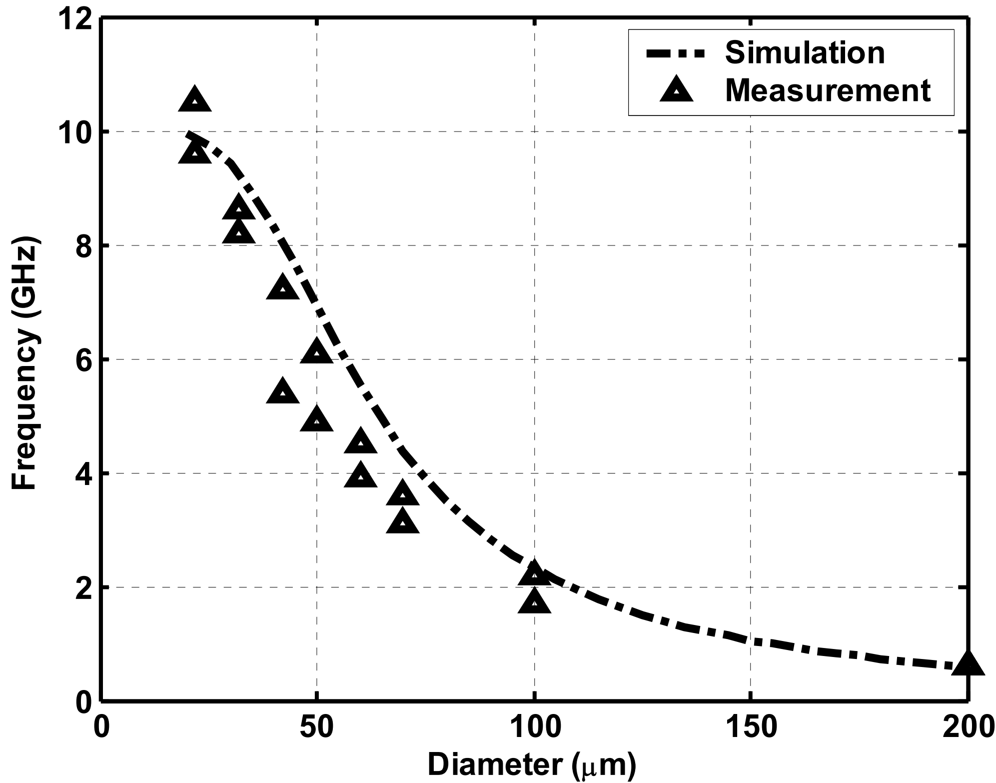

Fig. 11 3dB frequency for 22 μm through 200 μm diameter devices at 10V reverse bias with model for frequency limitation

3.5. Bit Error Rate Measurements

Several samples were prepared for packaging with Helix HXR2312 3.6 GHz 12 Channel Receiver arrays. The samples were sent to Helix in Zurich, Switzerland and were bonded to the Helix receiver array using 25 μm Gold wire wedge bonding. There were limitations in using this device but it was the only option for this testing. The first and perhaps most important limitation is the mismatch input impedance of the Helix amplifier. The Helix amplifier is designed to have a matched capacitive load of 450 fF, the typical capacitance of Optospeed InGaAs photodetectors which is the typical photodetector used in the optical interconnect standard. Our photodetectors have a 70fF capacitance. One other draw back is that even though the specification mentioned earlier called for 30 to 80 μm diameter photodetectors the testing was done with 50 μm core multi-mode fiber (MMF). This means that the 42 μm photodetector was only capturing 70% of the incident light at best.

The photodetectors were tested with the Helix receiver to measure the bit error rate BER and the eye-diagram. The photoreceiver was tested using an HP8664A Synthesized Signal Generator connected to a HP70841B Pattern Generator which was connected to a laser driver and a New Focus Model-1780 850nm 10G Hz Laser Diode, which was coupled to MMF and sent through an EXFO FVA-3100C Variable Attenuator. The output fiber of the Variable Attenuator was butt-coupled with the photodetector by line of sight and by maximizing the received photocurrent. The receiver is then connected to a HP70842B Error Detector to measure BER and a Agilent infinium DCA Wide Bandwidth Oscilloscope with HP54743A TDR Module to measure the eye-diagram. During the test the photodetector is biased at 1.8V reverse bias.

The HP70841B Pattern Generator was setup to send a PRBS 2^{23}-1 sequence to laser diode with a clock frequency of 1 GHz, 1.5 GHz, 2 GHz and 3 GHz on four separate runs. BER was measured using the HP70842B Error Detector which had the same pseudo random bit sequence (PRBS) 2^{23}-1 programmed for comparison. The BER was measured as a function of power by controlling the attenuation factor on the calibrated EXFO FVA-3100C Variable Attenuator. Fig. 12 shows the measured BER from a randomly selected detector in a 12x1 array. Ideal "error free" transmission is considered to be 1 part in 1 trillion or a BER of 10^{-12}. At 3 GHz the Si-RCE photodetector was able to achieve a BER of 10^{-12} at -6.5 dBm an order of magnitude worse than Optospeed's InGaAs photodetectors which require -16.5 dBm at the same BER.

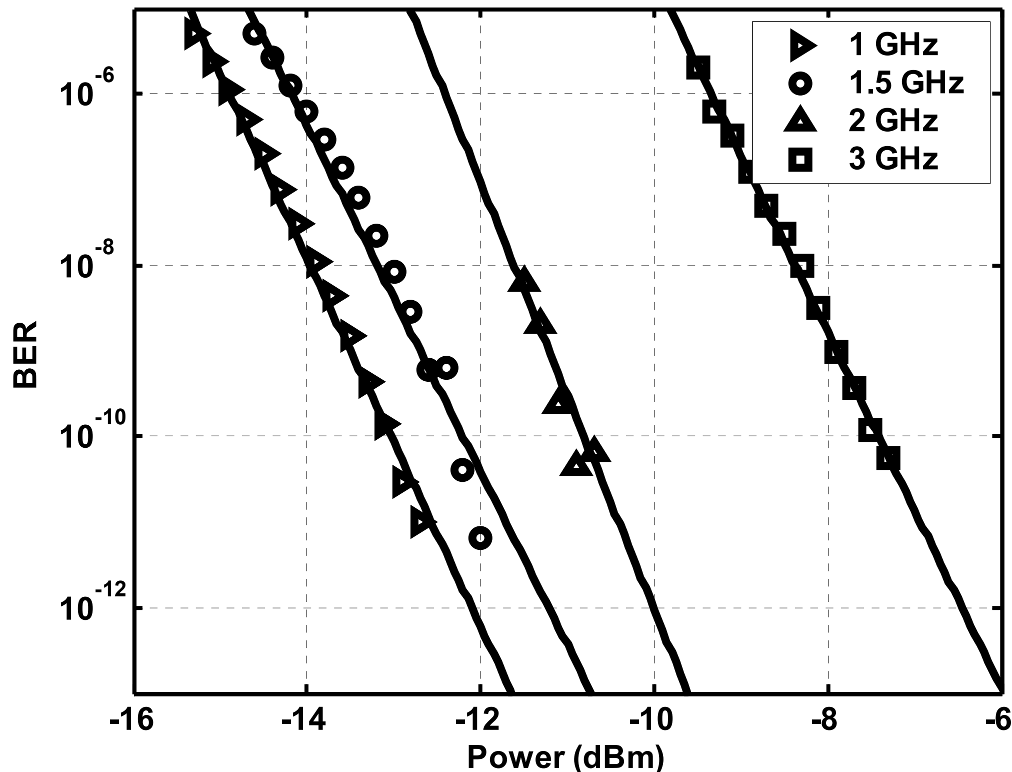

Fig. 12 Bit Error Rate measurement on single detector in 12x1 photodetector array

The other thing to note in Fig. 12 is the 5.5 dBm shift in minimum received power for 1 GHz transmission to 3 GHz transmission. The designers at Helix felt that this shift in minimum received power is due to the mismatched load of the receiver on the photodetector caused by the lower capacitance. The other cause of an increase in minimum received power, at all frequencies, is the problem of not collecting all the light from the MMF as well as the reduced responsivity at 850 nm because of misaligned spectral peak.

3.6. Eye Diagram

Eye diagrams show the accumulated response to a PRBS. They are used to measure the jitter in a received signal which can be described as the high frequency fluctuation of the signal from its ideal position. For communication standards masks are defined for the eye diagrams that declare regions off limits, and if the signal should fall within the region then the device would fail the standards certification. Typically eye diagrams are measured on a photodetector connected to a transimpedance amplifier with a fixed gain. Therefore at higher frequencies a lowering of the output magnitude will occur due to 3dB roll off. The Helix HXR2312 has a rail-to-rail limiting amplifier built in which means the magnitude of the output is constant for changing input magnitudes. Therefore the usefulness of the eye diagrams is questionable in this study as it can only reasonably measure the lateral eye opening due to diffusing carriers. Fig. 13 shows the eye-diagram for the same randomly selected detector in a 12x1 array used in the BER results. The eye shows good opening at 3 GHz and -9.5 dBm optical power. The plot does not show any characteristic signs of long diffusion tails.

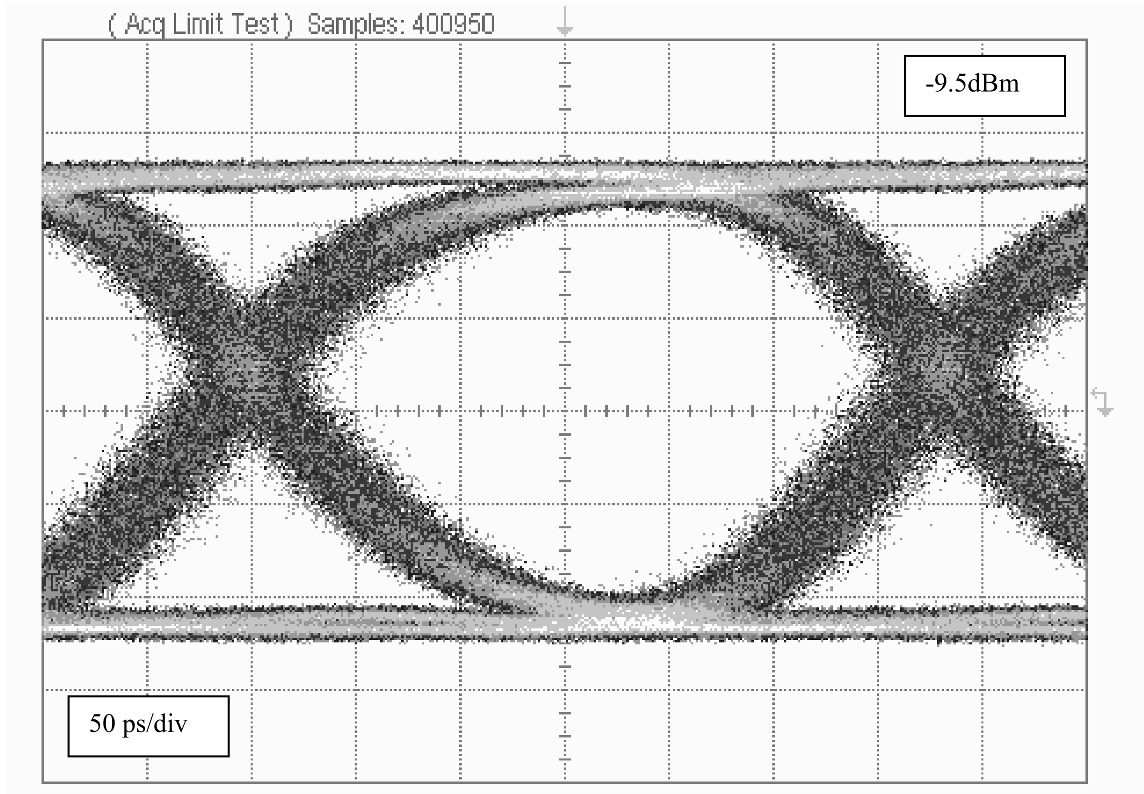

Fig. 13 Eye Diagram for single photodetector in 12x1 array at 3 GHz

4. CONCLUSIONS & FUTURE WORK

This work has presented commercially reproducible Si substrates with buried distributed Bragg reflectors, having reflectivity over 90%, used to fabricate Si-RCE *p-i-n* photodetectors capable of responsivity above 0.3 A/W and bandwidth in excess of 10 GHz. Photodetector arrays were fabricated and wire bonded with existing Si based receiver circuits to make an all-Si photoreceiver operating at 3 GHz, showing performance that could soon compete with existing compound semiconductor photodetectors for a fraction of the cost. The wafers could also be used to fabricate a host of Si based integrated optoelectronics owing to the availability of Si processing and the availability of large wafer sizes. These wafers are well suited for large scale integration and are compatible with standard CMOS processing making them ideal for fabricating photodetectors monolithically with receiver circuits.

The benefit of an RCE structure is to increase the efficiency for a given absorption thickness detector while maintaining the bandwidth. The drawback of the RCE structure, however, is the wavelength selectivity of the photodetector efficiency. To counteract this selectivity and yet still benefit from the RCE structure one can coat the top surface of the detector with an anti-reflection (AR) coating which will result in a "two-pass" detector where the light enters the photodetector and reflects off the buried mirror resulting in two passes of the absorption length. This will increase efficiency over a conventional detector by nearly two-fold while keeping the wavelength insensitivity over a substantial range. Fig. 14 shows the simulated responsivity-wavelength dependence of different absorption thicknesses as well as an 8 μm thickness with an AR coating showing the wavelength insensitivity around 850 nm.

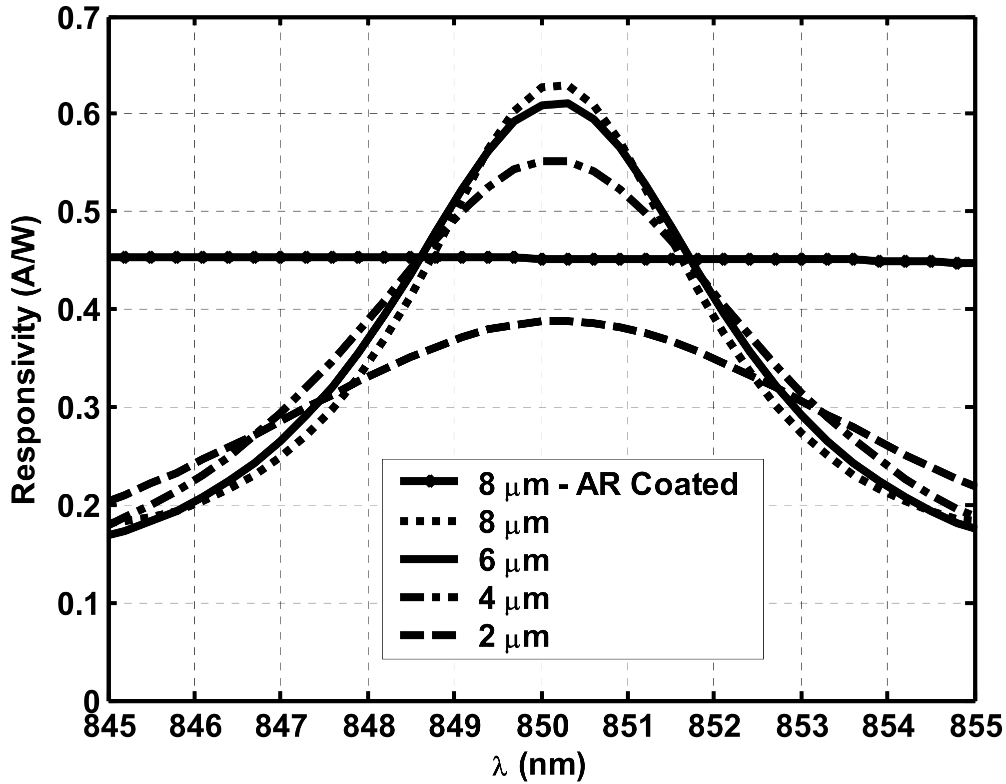

Fig. 14. Simulated responsivity for RCE Photodetectors of different absorption lengths as well as 8 μm "two-pass" photodetector

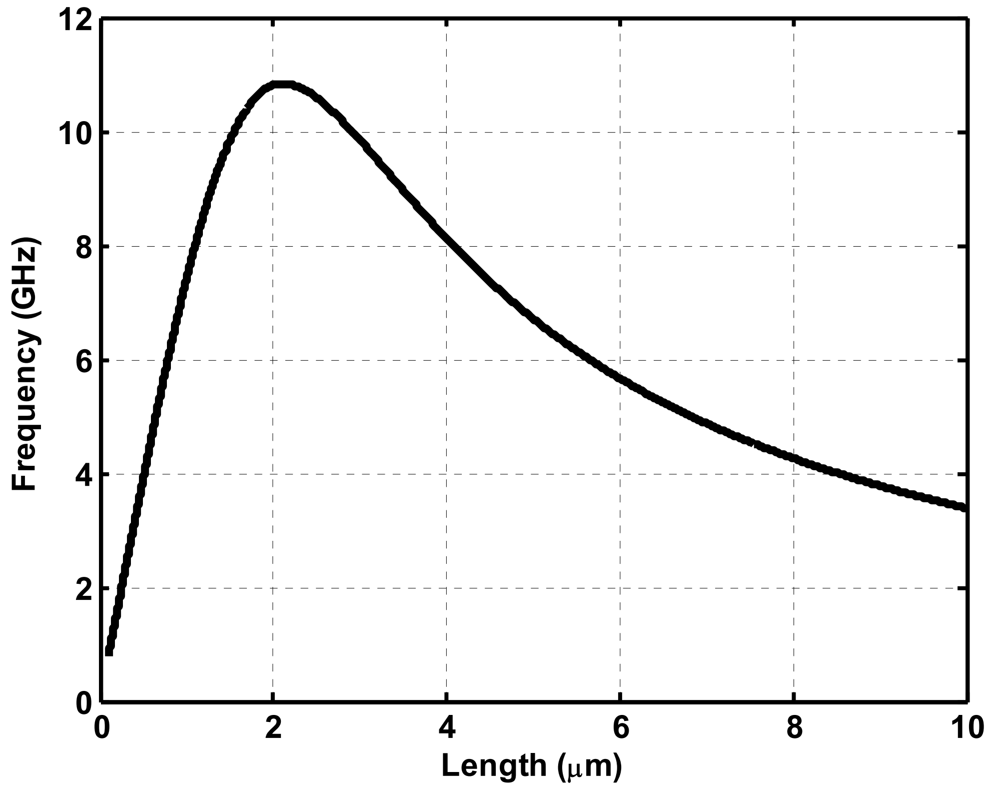

Fig. 15. Simulated 3 dB bandwidth of an 80 μm-diameter photodetector with 1.8V reverse bias

Just as increasing the absorption length will increase the efficiency, decreasing the absorption length will increase the bandwidth due to the reduction of carrier transit time. This effect is limited, however, as decreasing the absorption thickness will cause the photodetector capacitance between the *n* and *p* contacts to increase, resulting in the degradation of the device bandwidth. The goal of the designer is to find the optimal point for absorption length where capacitance and carrier transit time are minimized. The transit time of photodetectors is a function of the device length and the applied bias, as there is a relationship between carrier velocity and applied field. Fig. 15 shows the 3 dB bandwidth of an 80 μm-diameter detector with 1.8 V reverse bias.

ACKNOWLEDGEMENTS

The authors wish to thank Mike Ameen and Mark Harris at Axcelis Technologies for providing ion-implantation services for this project. We would also like to thank Philippe Flückiger and the entire staff at the Center of Microtechnology at EPFL for help in the fabrication of these detectors. Additionally we would like to thank Bruno Ghyselen of SOITEC SA for fabrication of the double SOI wafers. The authors also thank Martin Bossard and Jörg Wieland of Helix AG for packaging our detectors with their receiver circuits as well as for doing the BER and Eye-diagram testing.

This research was sponsored by the Army Research Laboratory (ARL) and was accomplished under the ARL Cooperative Agreement Number DAAD17-99-2-0070. The views and conclusions contained in this document are those of the authors and should not be interpreted as representing the Laboratory or the U.S. Government.

REFERENCES

[1] P. E. Green, "Paving the Last Mike With Glass", *IEEE Spectrum*, December 2002, pp. 13-14.
[2] B. Yang, J. D. Schaub, S. M. Csutak, D. L. Rogers, and J. C. Campbell, "10-Gb/s All-Silicon Optical Receiver," *IEEE Photonics Technology Letters*, Vol. 15, No. 5, May 2003, pp. 745-747.
[3] Optospeed, "PDCA12-68 12 Channel InGaAs p-i-n photodiode specification sheet," http://www.optospeed.com/, December 2002.
[4] UDT Sensors Inc., "PIN-UHS016 Ultra High Speed Si photodiode specification sheet," http://www.udt.com/, December 2002.
[5] M. K. Emsley, O.I. Dosunmu, and M. S. Ünlü, "Silicon Substrates With Buried Distributed Bragg Reflectors for Resonant Cavity-Enhanced Optoelectronics," *IEEE Journal of Selected Topics in Quantum Electronics*, Vol. 8, No. 4, July/August 2002, pp. 948-955.
[6] M. K. Emsley, O.I. Dosunmu, and M. S. Ünlü, "High-Speed Resonant-Cavity-Enhanced Silicon Photodetectors on Reflecting Silicon-on-Insulator Substrates," *IEEE Photonics Technology Letters*, Vol. 14, No. 4, April 2002, pp. 519-521.
[7] Infineon Tecnologies, "Parallel Optical Links (PAROLI)," http://www.infineon.com/paroli/, July 2003.
[8] M. Gökkavas, G. Ulu, O. Dosunmu, R. P. Mirin, and M. S. Ünlü, "Resonant Cavity Enhanced Photodiodes with a Broadened Spectral Peak," *Proceedings of IEEE Lasers and Electro-Optics Society 2001 Annual Meeting,* Vol. 2, pp. 768-769, November, 2001.